Robotica (2018) volume 36, pp. 1728–1742. © Cambridge University Press 2018
doi:10.1017/S026357471800067X

Sliding mode nonlinear disturbance observer-based adaptive back-stepping control of a humanoid robotic dual manipulator

Keqiang Bai[1,*], Xuantao Gong[2,*], Sihai Chen[3], Yingtong Wang[4] and Zhigui Liu[1,*]

[1]*School of Information Engineering, Southwest University of Science and Technology, Mianyang 621010, P.R. China*
[2]*Information Technology Teaching Center, Tianfu College of Southwestern University of Finance and Economics, Mianyang 621000, P.R. China*
[3]*Science and Technology Department, Mianyang Vocational and Technical College, Mianyang 621000, P.R. China*
[4]*School of Civil and Environmental Engineering, City College of Southwest University of Science and Technology, Mianyang 621000, P.R. China*
E-mails: sihai_chen@63.com, 462806425@qq.com

(Accepted July 11, 2018. First published online: August 7, 2018)

SUMMARY
An adaptive back-stepping sliding mode controller (ABSMC) algorithm was developed for nonlinear uncertain systems based on a nonlinear disturbance observer (NDO). The developed ABSMC was applied to attitude control for the dual arm of a humanoid robot. Considering the system uncertainty and the unknown external disturbances, the ABSMC scheme was designed to eliminate the chattering phenomenon in the traditional sliding mode control and to reduce the tracking error closer to zero. The ABSMC algorithm solved problems related to the chattering of the system for both uncertainties and disturbances in the humanoid robotic system with an NDO in a two-dimensional environment. The algorithm was designed to work equally well with agents, with higher degrees of freedom in different applications. The method was appropriate for improving tracking performance. The ABSMC algorithm guaranteed global stability and improved the dynamic performance of the system. The algorithm inherited a low computational cost, probabilistic completeness, and asymptotic optimality from the fuzzy sliding mode control. This algorithm has a practical application in the dual arm of a humanoid robot with a circular trajectory. This paper showed the effectiveness and applicability of the proposed methods, which reduced the output of the controller and improved the control performance of the humanoid robotic system. The new combined control algorithm, ABSMC, was able to feasibly and efficiently weaken the chattering on the robot's closed-loop paths, starting and finishing at the same configuration.

KEYWORDS: Adaptive back-stepping sliding mode control, Humanoid robots, Nonlinear disturbance observer, Humanoid robotic system

1. Introduction

A robot control system is a typical, nonlinear multivariable, and strongly coupled complex system. Many uncertain factors are related to the robot in actual missions. Consequently, the controlled dual arm of the humanoid robotic system is difficult to operate. On the experimental platform, a stability inspection of the dual-arm robot control method is necessary. Many scholars have studied dual-arm robots, with areas of focus including modelling, control, and so on.[1,2] Tonke and Lee developed a Petri net model based on specific conditions for each step in the process and developed a transmission

* Corresponding authors. E-mail: baisir@mail.ustc.edu.cn, 35657861@qq.com, liuzhigui@swust.edu.cn

module to obtain optimal conditions for a sequence analysis. This method also demonstrated the two independent arms in a way that increased throughput.[1] Shin and Kim based the validation of the human-like movements of the controller on a virtual, dynamic model to manipulate objects with humanoid robotic arms.[2]

From a control perspective, trajectory tracking control in the sensorless part of the dual-arm humanoid robotic system was studied.[3–6] Phee *et al*. proposed a method to estimate the end-effector parameters using only a force and a position sensor at the proximal site.[3] Nicolis *et al*. employed a control framework for the sensorless execution of a force control task with an application for a lightweight dual-arm robot.[5] Ragaglia *et al*. introduced a novel approach based on an observer with a joint position, joint velocity, and electric current measure that did not rely on the dedicated hardware torque. This was due to the operator power and its ability to conduct arm movement experiments shown in an ABB's robotic dual-arm concept FRIDA.[6] These models could not reduce the complexity of programming arm exercises that required multiple tasks. The disadvantages of these models included a lack of accuracy, an inability to ensure the safety of the operator, and so on.

The dual-arm design is essentially an interaction of these models, under specific circumstances with their environment to monitor interference. In the field of modern control, many studies on these types of mechanical arm systems have used the sliding mode control (SMC),[7–9] the internal uncertainty (operator),[10–12] and/or the external interference (between the manipulator and the environment).[10,12] Liu *et al*. introduced a nominal, linear time-invariant system, considering the real system as the nominal one with uncertainties, including parameter perturbations, nonlinear time-varying uncertainties, and external disturbances,[13] and they designed a nominal controller based on the optimal control method for the nominal system to achieve the desired tracking properties. Although this paper adopted the sliding mode design, it had nothing to do with disturbance but could bring jitter to the control system. It is necessary to ensure that the nonlinear system is robust enough to solve the jitter problems of the SMC. This paper proposed a control method based on a nonlinear disturbance observer (NDO).[14] An NDO is designed as an observer of friction, which changes quickly and, sometimes, discontinuously.[14] An adaptive design was proposed to solve the challenge of the internal uncertainties and the external disturbances of the nonlinear system of the compound disturbance.

An SMC is very robust, has fast corresponding characteristics, and is therefore an ideal tool to process a mixed system coupling.[15] However, the SMC process is divided into continuous and discontinuous parts. The discontinuous part ensures that synovial control occurs during the process of shaking. The boundary layer limit reduces the SMC jitter problem to address this issue. However, the controller of the tracking accuracy is reduced.[16,17] In contrast, the upper bound of the disturbance is usually unknown. Therefore, the SMC switch gain should be large enough to guarantee system stability. The results of a previous study showed that the adaptive fuzzy logic could be used to approximate the SMC switch gain and effectively reduce the jitter of the system.[18] Therefore, the SMC combined with the fuzzy logic proved to be effective in the machine control tool process.

The design followed an adaptive back-stepping sliding mode controller (ABSMC) algorithm with the support of a system offering steady-state performance. The NDO[19–25] was used to address the disturbances. The problem of controlling a cooperative robotic system with kinematic and dynamic uncertainties was analysed as a synchronizing problem in recent studies.[26,27] A Lyapunov analysis was used to justify the closed-loop stability and the exponential convergence of internal signals. This paper focused on the systemic existence of uncertainties and external disturbances within the dual arm of a humanoid robot. The paper also focused on the NDO, which observed system uncertainties and disturbances by selecting design parameters. As a result, the NDO gave the observer exponential convergence. For introducing the ABSMC system, the NDO was used to design the controller to ensure that it was robust to unknown uncertainties and external disturbances as well as to ensure the stability and security of the system runtime of the humanoid robotic arms. This paper proposed a method to inhibit the chattering of the ABSMC. The main reasons for the sliding mode chattering were the inappropriate choice of switch gain and the switching characteristics of the controller. In this paper, a sliding mode NDO was used to adjust the switch gain of an online adjustment to avoid excessive chattering due to the choice of switch by compensating for uncertainty. Therefore, softening the switching characteristics of the system suppressed the chattering effectively.

This paper presented an ABSMC control method to manipulate an object with a humanoid robotic arm that grabbed objects independently. The paper proposed the dual-arm system model based on the NDO of the ABSMC method to describe object manipulation features. The paper also provided the simulation and experimental results, where humanoid robotic procedures were used to validate the method.

https://doi.org/10.1017/S026357471800067X Published online by Cambridge University Press

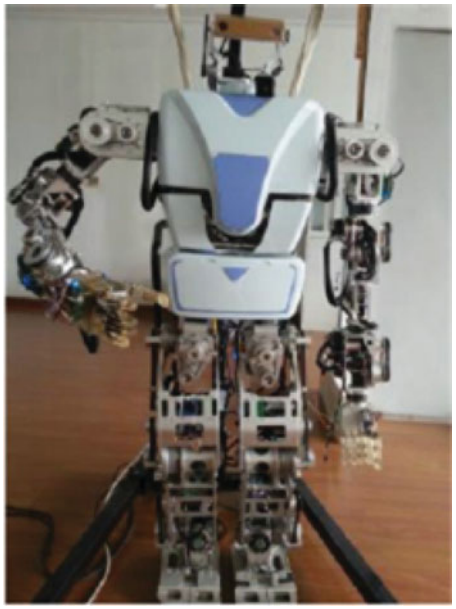

Fig. 1. Left- and right-arm postures of two different mechanical arms.

2. ABSMC Design

The ABSMC algorithm was proposed after considering the dynamic model of parameter uncertainty and external disturbance of humanoid robots. This control algorithm consisted of an ABSMC with adaptive parameters for a class of systems satisfying some conditions, where the upper bounds of the uncertainties were unknown.

2.1. System description

The motor features of a seven degrees-of-freedom (DOF) dual-arm humanoid robotic system were considered as the research object, as shown in Fig. 1.

The description of the system can be expressed as follows:

$$\begin{cases} \dot{x}_1 = x_2 \\ \dot{x}_2 = \frac{K_t}{M_t} x_3 - \frac{B}{M_t} x_2 + \frac{N}{M_t} \sin(x_1) + d_2(x,t) \\ \dot{x}_3 = -\frac{R}{L} x_3 - \frac{K_b}{L} x_2 + \frac{1}{L} u - \frac{1}{L} d_3(x,t) \end{cases} \tag{1}$$

where x_1, x_2, x_3, and u denote the position of the mechanical arm, the velocity of the mechanical arm, the electric current of the motor, and the input of the system, respectively. $y = x_1$ is the output of the system. $d_2(x,t)$ denotes the parameter uncertainty, and $d_3(x,t)$ denotes the parameter uncertainty and external disturbance. Table I shows the meaning of the other parameters and the nominal value.

In this paper, the control target was the output tracking the input command $y_d = \sin(t)$. To achieve control objectives, it was assumed that the input command y_d and its two derivatives existed and were bounded, and $d_i(x,t)$ was bounded to unknown uncertainties. Therefore, $d_i(x,t) < \bar{d}_i$, where $\bar{d}_i$ is known. The humanoid robotic system was a single input and single output, and the system was in an observable state.

2.2. NDO design

The basic design concept was to modify the estimates of the difference between the output and the actual output. The disturbance observer was introduced to approach the disturbance of the system to reduce the influence of the external disturbances on the system and to improve the control precision of the system. The NDO, which was simple in structure and computational complexity, did not need to assume that a complex disturbance was extremely slow. The restriction of the rate of the complex disturbance was relaxed, and a high precision estimation was obtained. The disturbance observer is

https://doi.org/10.1017/S026357471800067X Published online by Cambridge University Press

Table I. 7-DOF humanoid robotic arm parameters.

Parameter	Physical meaning	Value
K_t (N · m/A)	Torque coefficient	1
M_t (kg · m^2)	Rotational inertia	0.0513
B (N · m · s/rad)	Viscosity coefficient of friction	0.015
N (N · m)	Mechanical arm's motor torque	0.3528
R (Ω)	Resistance	0.075
K_b (N · m/A)	Electromagnetic induction coefficient	0.085
L (H)	Inductance	0.001

designed as follows:[14]

$$\dot{\hat{d}} = -\boldsymbol{L}(\boldsymbol{q}, \dot{\boldsymbol{q}})\hat{d} + \boldsymbol{L}(\boldsymbol{q}, \dot{\boldsymbol{q}})(\boldsymbol{M}(\boldsymbol{q})\ddot{\boldsymbol{q}} + \boldsymbol{G}(\boldsymbol{q}, \dot{\boldsymbol{q}}) - \boldsymbol{\tau}) \tag{2}$$

where $\hat{d}$ is the internal state vector of NDO, $\boldsymbol{M}(\boldsymbol{q})$ is the symmetric positive definite, $\boldsymbol{G}(\boldsymbol{q}, \dot{\boldsymbol{q}})$ is the gravitational force vector, $\boldsymbol{\tau}$ is the control vector, and $\boldsymbol{L}$ is the nonlinear equation. This can be expressed as follows:

$$\boldsymbol{L}(\boldsymbol{q}, \dot{\boldsymbol{q}})\boldsymbol{M}(\boldsymbol{q})\ddot{\boldsymbol{q}} = \begin{bmatrix} \dfrac{\partial \boldsymbol{T}(\boldsymbol{q}, \dot{\boldsymbol{q}})}{\partial \boldsymbol{q}} & \dfrac{\partial \boldsymbol{T}(\boldsymbol{q}, \dot{\boldsymbol{q}})}{\partial \dot{\boldsymbol{q}}} \end{bmatrix} \begin{bmatrix} \dot{\boldsymbol{q}} \\ \ddot{\boldsymbol{q}} \end{bmatrix} \tag{3}$$

Let z denote an auxiliary variable vector:

$$z = \hat{d} - T(\boldsymbol{q}, \dot{\boldsymbol{q}}) \tag{4}$$

Hence, NDO is given as follows:

$$\dot{z} = -\boldsymbol{L}(\boldsymbol{q}, \dot{\boldsymbol{q}})z + \boldsymbol{L}(\boldsymbol{q}, \dot{\boldsymbol{q}})(\boldsymbol{G}(\boldsymbol{q}, \dot{\boldsymbol{q}}) - \boldsymbol{\tau} - T(\boldsymbol{q}, \dot{\boldsymbol{q}})) \tag{5}$$

According to Eqs. (4) and (5), the system NDO can be written as follows:

$$\begin{cases} \hat{d} = z + p(x_1, x_2) \\ \dot{z} = -L(x_1, x_2)z + L(x_1, x_2)(-p(x_1, x_2) - f - gu) \end{cases} \tag{6}$$

where $p(x_1, x_2)$ is needed to design the nonlinear function, and $L(x_1, x_2)$ is the gain of the nonlinear observer: $L(x_1, x_2)\dot{x}_2 = \mathrm{d}p(x_1, x_2)/\mathrm{d}t$.

By selecting the appropriate $L(x_1, x_2) > 0$, the observation error is based on the index of convergence.

2.3. Based on the NDO of the ABSMC design

Because of the uncertainty of the system and the disturbance, the controller output was higher and was made directly on the ABSMC system design. To solve this problem, instead of the observer being part of the compensation, a disturbance observer was designed for load disturbance on the system performance.

This paper proposed the NDO of the ABSMC scheme illustrated in Fig. 2, creating target tracking in the closed loop by shaping the robot system with the ABSMC position output. The proposed controller in the inner position control loop guaranteed an almost ideal tracking of this position reference. The following sliding mode controller and adaptation law is a representation of an NDO model that is used in the proposed control scheme.

The back-stepping method is derived from the sliding mode controller and the adaptation law. The Lyapunov function is expressed as follows:[28]

$$V = V_{n-1} + \frac{1}{2}s_n^2 \tag{7}$$

https://doi.org/10.1017/S026357471800067X Published online by Cambridge University Press

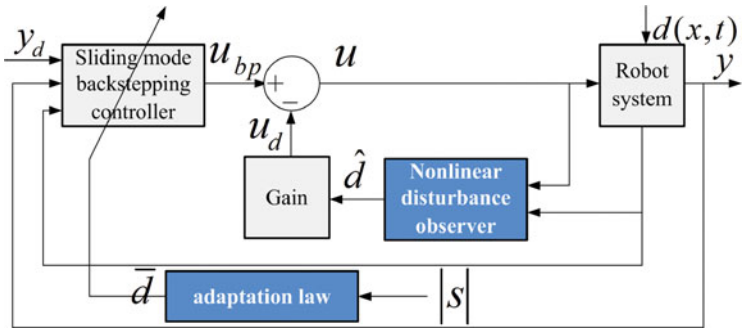

Fig. 2. Proposed control structure diagram.

For the third-order system, three state variables exist. Therefore, three sliding mode surfaces need to be defined as follows:

$$V = \frac{3}{2}s_1^2 + s_2^2 + \frac{1}{2}s_3^2 \tag{8}$$

where

$$s_i = x_i + \alpha_{i-1}\,(i = 1, 2, 3)$$

where s_i is a sliding surface vector, α_{i-1} is the state of the ideal value of x_i, and $\alpha_0 = y_d$.

Step 1: The first subsystem of system (1) is $\dot{\mathbf{x}}_1 = \mathbf{x}_2$, where $\mathbf{x}_2$ is a virtual input, and the derivative of the first sliding surface $s_1 = x_1 - y_d$ with respect to time is as follows:

$$\dot{s}_1 = \dot{x}_1 - \dot{y}_d = x_2 - \dot{y}_d = s_2 + \alpha_1 - \dot{y}_d \tag{9}$$

To make the first subsystem reach the surface of the sliding mode and to create movement on this surface, the virtual control law is defined as follows:

$$\alpha_1 = -k_1 s_1 + \dot{y}_d\,(k_1 > 0) \tag{10}$$

The derivative of the first sliding surface $V_1 = \frac{1}{2}s_1^2$ with respect to time is

$$\dot{V}_1 = s_1\dot{s}_1 = -k_1 s_1^2 + s_1 s_2 \tag{11}$$

Step 2: The derivative of the second sliding surface $s_2 = x_2 - \alpha_1$ with respect to time is

$$\begin{aligned}\dot{s}_2 = \dot{x}_2 - \dot{\alpha}_1 &= \frac{K_t}{M_t}x_3 - \frac{B}{M_t}x_2 + \frac{N}{M_t}\sin(x_1) + d_2(x,t) + k_1(s_2 + \alpha_1 - \dot{y}_d) - \ddot{y}_d \\ &= \frac{K_t}{M_t}(s_2 + \alpha_2) - \frac{B}{M_t}x_2 + \frac{N}{M_t}\sin(x_1) + d_2(x,t) + k_1(s_2 + \alpha_1 - \dot{y}_d) - \ddot{y}_d\end{aligned} \tag{12}$$

The virtual control law is defined as follows:

$$\alpha_2 = -k_2 s_2 - \frac{M_t}{K_t}s_1 + \frac{B}{K_t}x_2 - \frac{N}{K_t}\sin(x_1) - \frac{M_t}{K_t}d_{\Delta 2}\mathrm{sgn}(s_2) + \frac{M_t}{K_t}k_1\dot{y}_d + \frac{M_t}{K_t}\ddot{y}_d \tag{13}$$

where

$$\mathrm{sgn}(s_2) = \begin{cases} 1 & s_2 > 0 \\ 0 & s_2 = 0 \\ -1 & s_2 < 0 \end{cases}, \quad d_{\Delta 2} = \bar{d}_2$$

https://doi.org/10.1017/S026357471800067X Published online by Cambridge University Press

Equation (13) is nondifferentiable. Therefore, Eq. (13) is modified as follows:

$$\alpha_2 = -k_2 s_2 - \frac{M_t}{K_t} s_1 + \frac{B}{K_t} x_2 - \frac{N}{K_t} \sin(x_1) - \frac{M_t}{K_t} d_{\Delta 2} \frac{\mu_2 s_2}{\sqrt{s_2^2 + \xi_2^2}} - \frac{M_t}{K_t} k_1 \dot{y}_d + \frac{M_t}{K_t} \ddot{y}_d \tag{14}$$

where μ_2 and ξ_2 are constants for the design $\mu_2 > 1$ and $0 < \xi_2 < 1$, respectively.

The derivative of the second sliding surface $V_2 = V_1 + \frac{1}{2} s_2^2$ with respect to time is

$$\dot{V}_2 = \dot{V}_1 + s_2 \dot{s}_2 = -k_1 s_1^2 + s_1 s_2 + s_2 \dot{s}_2 \tag{15}$$

Now, the derivative of the second sliding surface is substituted as a sliding surface derivative (12) into Eq. (15). This yields the following:

$$\dot{V}_2 = \dot{V}_1 + s_2 \dot{s}_2 = -k_1 s_1^2 + s_1 s_2 + s_2 \dot{s}_2 = -k_1 s_1^2 + s_1 s_2 - |s_2| \, d_{\Delta 2} \left(\frac{\mu_2 |s_2|}{\sqrt{s_2^2 + \xi_2^2}} - 1 \right) \tag{16}$$

Using the aforementioned NDO and the structural diagram in Fig. 2, the third subsystems of system (1) can be written as

$$\dot{x}_3 = -\frac{R}{L} x_3 - \frac{K_b}{L} x_2 + \frac{1}{L}(u_{bp} - u_d) - \frac{1}{L} d_3(x, t) = f(x_2, x_3) + g(u_{bp} - u_d) + d = f + g u_{bp} + \bar{d} \tag{17}$$

where $f = f(x_2, x_3) = -\frac{R}{L} x_3 - \frac{K_b}{L} x_2$, $g = \frac{\hat{d}}{u_d} = \frac{1}{L}$, and $\bar{d}$ is the observation error of the NDO $\bar{d} = d - \hat{d}$.

Step 3: The adaptation law was designed as follows:

$$\dot{s}_3 = \dot{x}_3 - \dot{\alpha}_2 = -\frac{R}{L} x_3 - \frac{K_b}{L} x_2 + \frac{1}{L} u - \frac{1}{L} d_3(x, t) - \dot{\alpha}_2 \tag{18}$$

$$u_{bp} = \frac{1}{g}(-k_3 s_3 - s_2 - f + \dot{\alpha}_2(x_1) + \dot{\alpha}_2(x_2) + \dot{\alpha}_2(y_d) - d_{\Delta 3} \mathrm{sgn}(s_3)) \tag{19}$$

Next, the disturbance observer for the third subsystem design is substituted into Eq. (1). Considering Eq. (6), the input to the controlled system is as follows:

$$u = u_{bp} - u_d = \frac{1}{g}(-k_3 s_3 - s_2 - f + \dot{\alpha}_2(x_1) + \dot{\alpha}_2(x_2) + \dot{\alpha}_2(y_d) - d_{\Delta 3} \mathrm{sgn}(s_3) - \hat{d}_3) \tag{20}$$

Now, the controlled system input (20) is substituted into Eq. (18) as follows:

$$\dot{s}_3 = -k_3 s_3 - s_2 - d_{\Delta 3} \mathrm{sgn}(s_3) + \bar{d}_3 \tag{21}$$

where $\bar{d}_3 = d_3(x, t) - \hat{d}_3$. The disturbance of the system reduces to $\bar{d}_3$ from $d_3(x, t)$. With the decrease in $\bar{d}_3$, the chattering of the system also reduces.

Step i ($3 < i \leq n$): Assume that we have designed virtual control laws α_j and defining $s_n = x_n - \alpha_{n-1}$, $j = 1, 2, 3, \ldots, i-1$. Computing the derivative of s_n

$$\begin{aligned} \dot{s}_n &= \dot{x}_n - \dot{\alpha}_{n-1} \\ &= g_0(\bar{x}_n) u + f_{n0}(\bar{x}_n) + d_n(\bar{x}_n, t) - \sum_{j=1}^{n-1} \frac{\partial \alpha_{n-1}}{\partial x_j} \dot{x}_j - \sum_{k=1}^{n-1} \frac{\partial \alpha_{n-1}}{\partial y_d^{(k)}} y_d^{(k+1)} \\ &= g_0(\bar{x}_n) u + f_{n0}(\bar{x}_n) - \sum_{j=1}^{n-1} \frac{\partial \alpha_{n-1}}{\partial x_j} (x_{j+1} + f_j(\bar{x}_j) - \sum_{k=1}^{n-1} \frac{\partial \alpha_{n-1}}{\partial y_d^{(k)}} y_d^{(k+1)} + d_{\Delta n}(\bar{x}_n, t) \end{aligned} \tag{22}$$

https://doi.org/10.1017/S026357471800067X Published online by Cambridge University Press

where $d_{\Delta n}(\bar{x}_n, t) = -\sum_{j=1}^{n-1} \frac{\partial \alpha_{n-1}}{\partial x_j} d(\bar{x}_j, t) + d_n(\bar{x}_n, t)$. Assume that we have $d_{\Delta n}(\bar{x}_n, t)$ bound and $|d_{\Delta n}(\bar{x}_n, t)| \leq \bar{d}_{\Delta n}$.

The time derivative of Eq. (7) provides the following Lyapunov function:

$$\dot{V} = \dot{V}_{n-1} + s_n \dot{s}_n \tag{23}$$

Using the above step, on the premise of meeting $|s_i| > \frac{\xi_i}{\sqrt{\mu_i^2 - 1}}$, the resulting expression of V is reduced to

$$\begin{aligned} \dot{V} &\leq -\sum_{j=1}^{n-1} k_j s_j + s_{n-1} s_n + s_n(-k_n s_n - s_{n-1} - -d_{\Delta n} \mathrm{sgn}(s_n) + \bar{d}_n) \\ &\leq -\sum_{j=1}^{n} k_j s_j - |s_n| d_{\Delta n} + s_n \bar{d}_n) \leq -\sum_{j=1}^{n} k_j s_j (n = 1, 2, 3;) \end{aligned} \tag{24}$$

As a result, the controller could be a stable system, and the NDO based on the ABSMC under the assumptions in Section 2.1 might remain uniformly and ultimately bounded. The range of the system error is $|s_i| \leq \frac{\xi_i}{\sqrt{\mu_i^2 - 1}}$.

From formula (24), we can obtain the following theorem.

Theorem. *Based on the input command y_d and its two derivatives being existing and bounded, and $d_i(x, t)$ was bounded to unknown uncertainties, and there were nonlinear disturbances in the observer and control laws, we know that all the signals in the closed-loop system are bounded and that the system is bounded and stable.*

3. Simulation Example

This paper proposed the NDO based on the ABSMC as a simulation. Next, the NDO sliding mode observer was designed. The NDO was used to estimate the matching interference for the dual arm of a humanoid robot. This paper designed a sliding mode observer to decrease the system's total interference, which would weaken the chattering of the SMC. The observers were challenging in this design. The simulation and experiments were based on a humanoid robotic manipulator with DC motor drives.

The aim of the repetitive control system was to run on a cycle of deviation after the first few cycles of learning; it could track the reference signal well. When the input signal, $r(t)$, is the bounded signal for the L period, it meets the following conditions:

1. $[I + C(s)P(s)K(S)]$ is regular.
2. $[I + C(s)P(s)K(S)]^{-1}$ is asymptotically stable.
3. $\|I - [I + C(s)P(s)K(S)]^{-1} C(s)P(s)\|_2 < 1$.

Here, I is the unit array, $K(S)$ is a feedforward item, $C(s)$ is the proportional-integration-derivative (PID) control item, and $P(s)$ is the open-loop transfer function of the system; in this case, the repetitive control system was stable, and the error was converged.

The method and the PID control were compared with repetitive control compensation to better display their effects and advantages. The comparison between the position tracking and the controller output of the proposed scheme as well as that of the PID control with repetitive control compensation is shown in Fig. 3.

As can be seen in Fig. 3(a), many position errors were observed in the beginning. However, Fig. 3(b) shows that with the controller algorithm, the error was almost close to zero. Fig. 3(c) and (d) shows that while a PID controller with repetitive control compensation was chattering, the ABSMC strategy, which was at the beginning of the first and second peaks, showed the chattering phenomenon. The reason for this result was that the SMC interfered with the sliding mode surface.

4. Experimental Results

Three experiments were performed on the arms[28] of the humanoid robots to verify the effectiveness of the proposed controller. The previously proposed adaptive robust controller with repetitive control compensation and the controller (ABSMC) proposed in this paper were compared.[29] In the first set

https://doi.org/10.1017/S026357471800067X Published online by Cambridge University Press

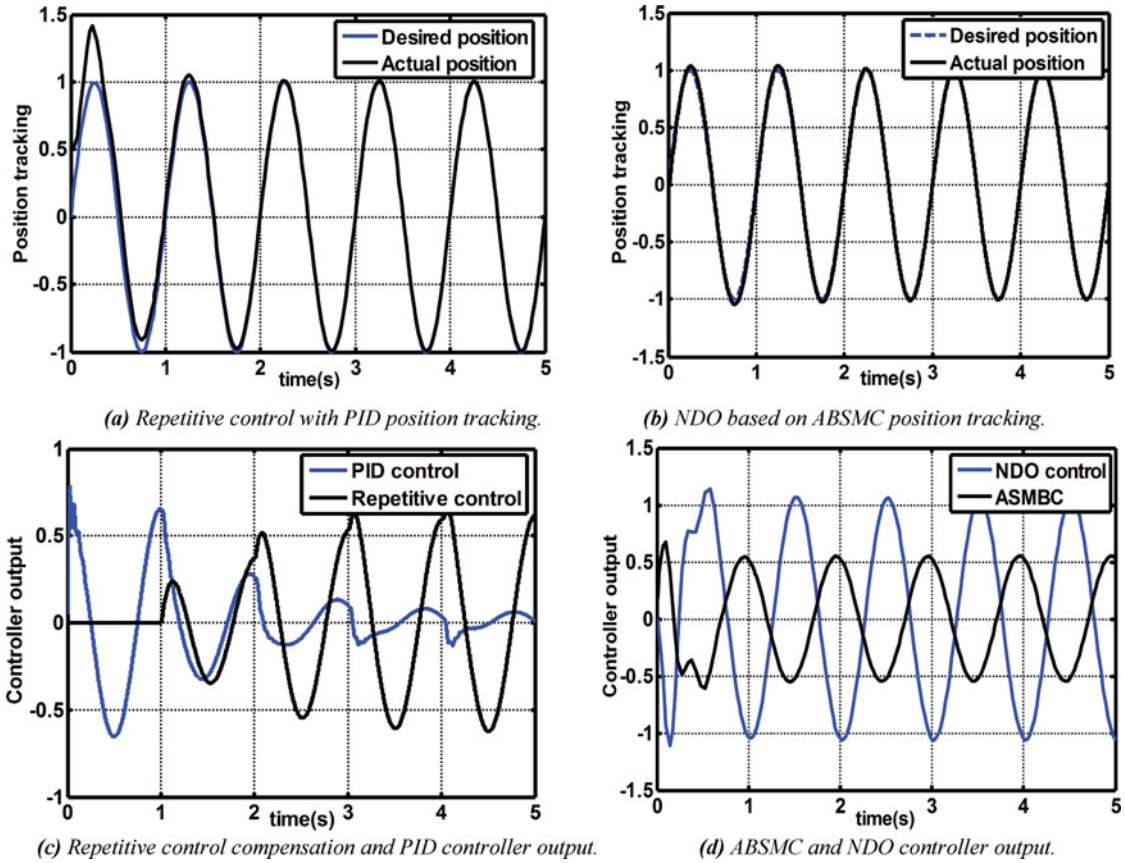

Fig. 3. Comparison of two control strategies. (a) Repetitive control with PID position tracking. (b) NDO based on ABSMC position tracking. (c) Repetitive control compensation and PID controller output. (d) ABSMC and NDO controller output.

of experiments, the trajectory in the Y-direction was considered under the effect of gravity. A more challenging double mechanical arm system test was used in the second experiment, which considered parameter uncertainty and external disturbances. The third experiment was a dual-arm moving object. The purpose of these experiments was to evaluate the performance of the proposed controller structure and the stability of the robotic system.

In the first experiment, a circular trajectory radius of 1 m was considered, as follows:

$$\begin{cases} x_r = 1.0\cos(0.02\pi t)\,u(t-2) \\ y_r = 1.0\sin(0.02\pi t)\,u(t) \end{cases}$$

where $u(t)$ denotes the unit step function. Circular trajectory tracking was adopted in the experiment; in the XY-plane, circular trajectory tracking was done through three focal points around the implementation of the algorithm. Subsequently, the mechanical arm was set for three points in the planar coordinates of (0–1000) mm, (0–1000) mm, and (0, 1000) mm. The entire process of the task time design took 12 s. Figure 4 shows the specific task execution.

Figure 5(a) shows the results of the repetitive control of the PID controller in tracking the desired trajectories in the XY-plane. The solid red line tracks the desired trajectories. At the same time, the dashed line portrays the actual results. As shown in the figure, in the process of controller trajectory tracking, the repetitive control of the PID controller was not appropriate because of the lack of consideration for the dynamic effect on the controller structure. In this case, the angular and linear velocities of the system error were relatively high, as shown in Fig. 5(b), because the actuators were affected by the change in the Coulombic force. Figure 6(a) verifies the effectiveness of the proposed ABSMC controller to track the desired trajectory. Based on the adaptive parameter design, the controller capitalized on combining the SMC, the back stepping for uncertainty, the offset of the

https://doi.org/10.1017/S026357471800067X Published online by Cambridge University Press

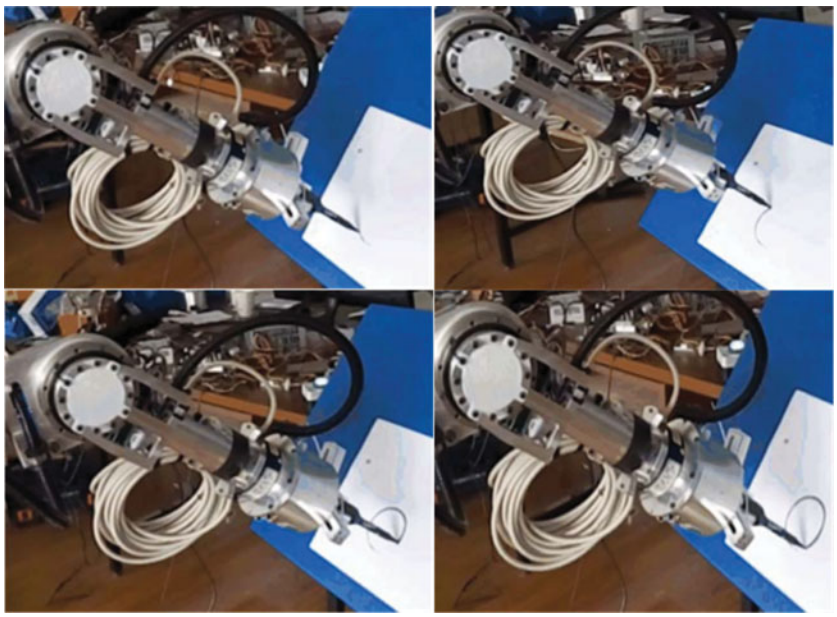

Fig. 4. Circular trajectory tracking process.

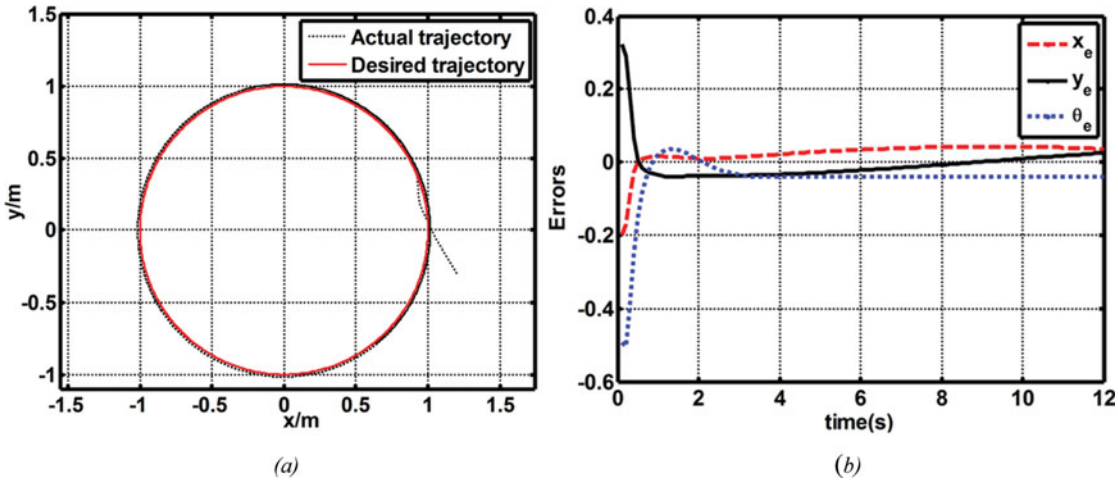

Fig. 5. Repetitive control with the PID trajectory tracking and the error chart.

structural uncertainty, and the parameters to provide appropriate tracking performance. Figure 6(b) shows that the angular and linear velocities of the system error were relatively small and that the convergence was better. Figure 6(b) shows that the error in the tracking performance was reduced compared with Fig. 5(b). Therefore, the ABSMC was more robust using the proposed method than using repetitive control with the PID method.

The second experiment considered the following system output trajectory tracking with the dual arm of a humanoid robot. The experiment was performed on the 7-DOF dual arm of a humanoid in the actual task environment. This robot was given the task of moving a plastic box. The experimental system and the system parameter selection[28] were as follows:

$$\begin{cases} \dot{x}_1 = x_2 \\ \dot{x}_2 = M^{-1}(x_1)\left[u - N(x_1, x_2)x_2 - G(x_1) + d(t)\right] \\ y = x_1 \end{cases}$$

where $G(x_1) \in R^2$ denotes the gravity vector and $d(t) \in R^2$ denotes the external disturbance. Figure 7 shows that the humanoid robot was given the special task of opening a door.

https://doi.org/10.1017/S026357471800067X Published online by Cambridge University Press

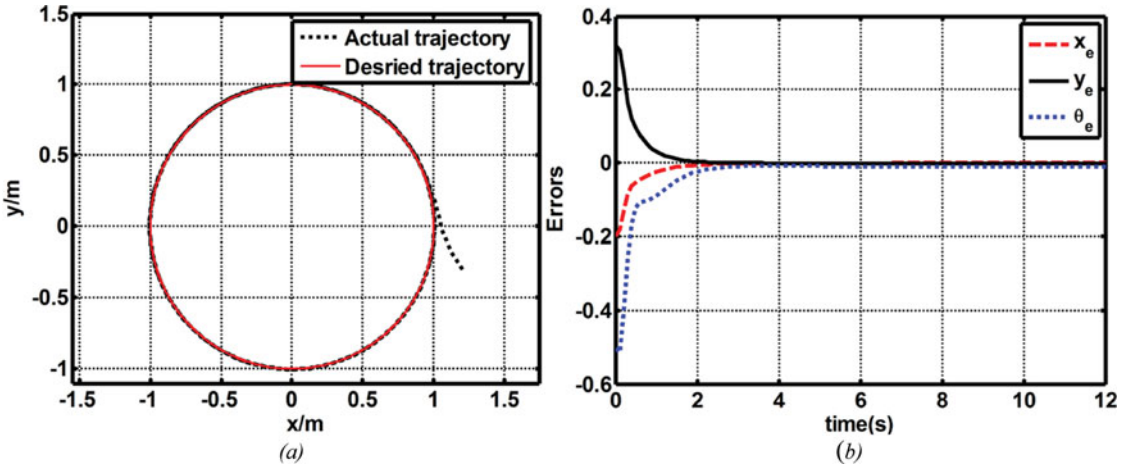

Fig. 6. The proposed controller ABSMC trajectory tracking and the error chart.

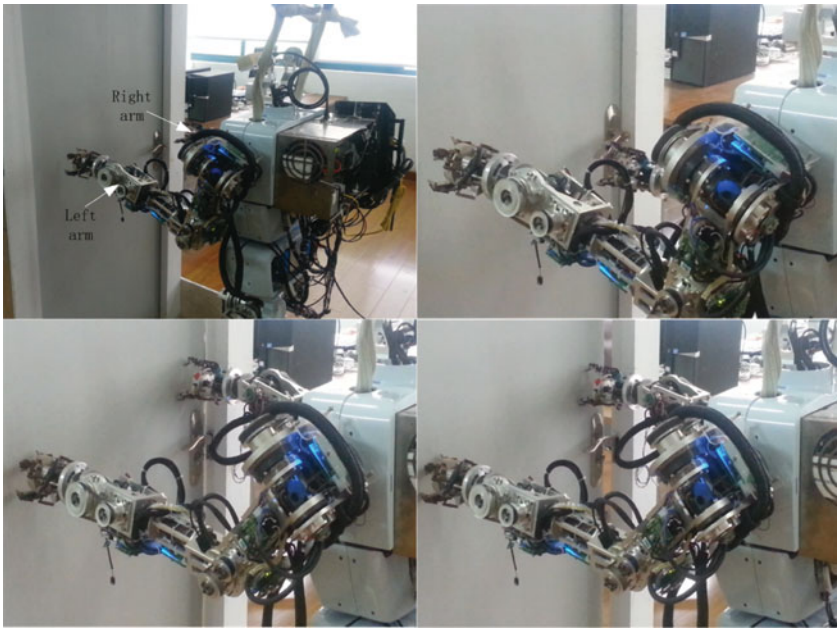

Fig. 7. Mechanical arm test process—opening a door.

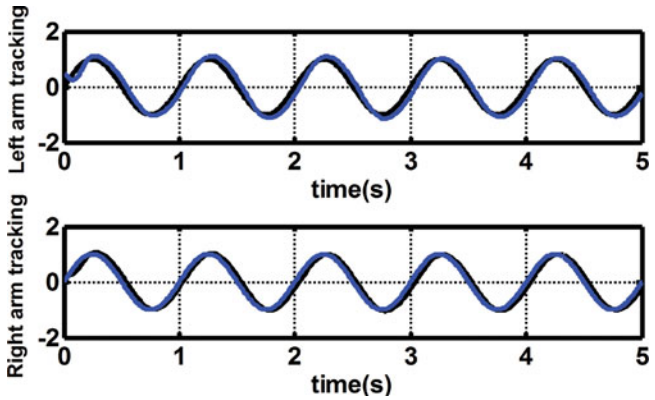

Fig. 8. Mechanical arm position tracking system.

https://doi.org/10.1017/S026357471800067X Published online by Cambridge University Press

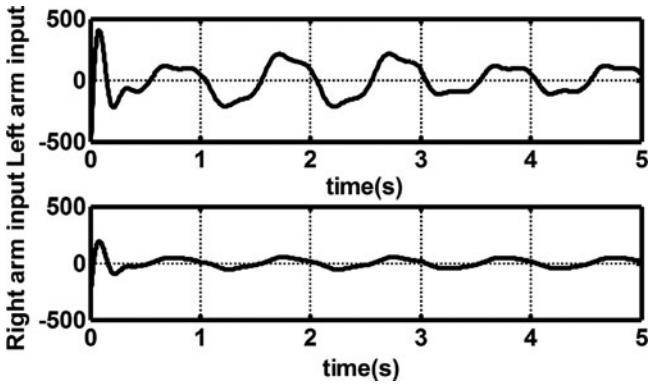

Fig. 9. Mechanical arm controller input.

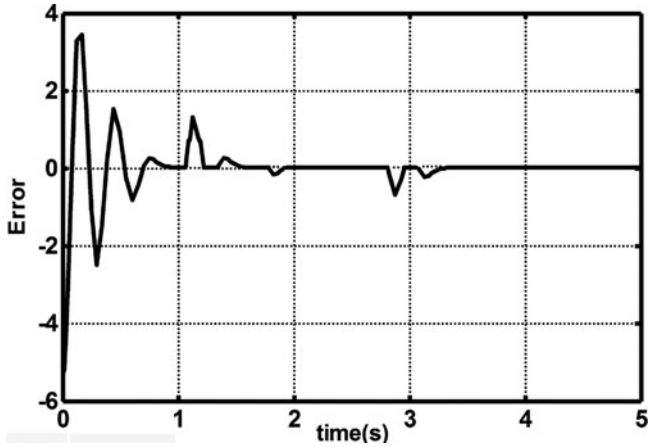

Fig. 10. Left-arm position tracking output error.

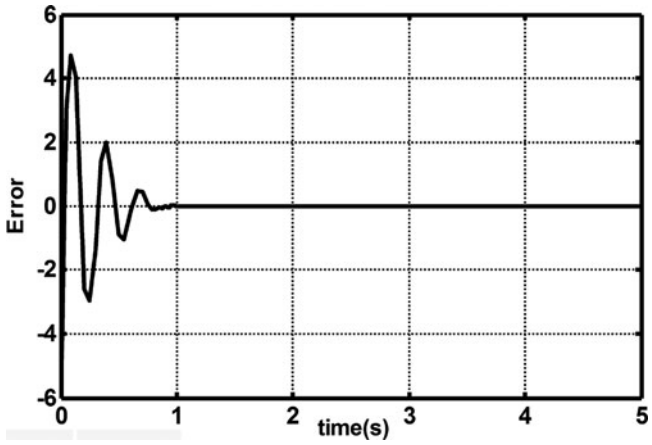

Fig. 11. Right-arm position tracking output error.

Figures 8–12 show the experimental results. In this case, parameters $M(x_1)_{11}$ during the $1 \leq t \leq 3$ have $1\text{kg} \cdot \text{m}^2$ fluctuations, and $d = 2$ is the external disturbance. Figure 8 shows the arms of the tracking trajectory around the system positions. The left arm, in the case of a disturbance, portrayed an obvious deviation from the desired tracking trajectory. The mechanical arm controller input is shown in Fig. 9. Figures 10 and 11 demonstrate the left and right arms under interference and no interference, respectively. The observer is the error value of the observed position system output. This figure clearly shows that the left arm adds interference, which can be viewed by the observer, and

https://doi.org/10.1017/S026357471800067X Published online by Cambridge University Press

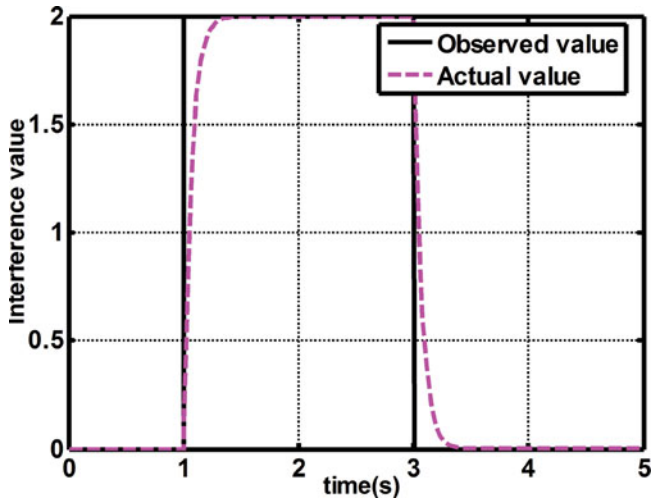

Fig. 12. NDO of adaptive back-stepping sliding mode control actual interference and observations.

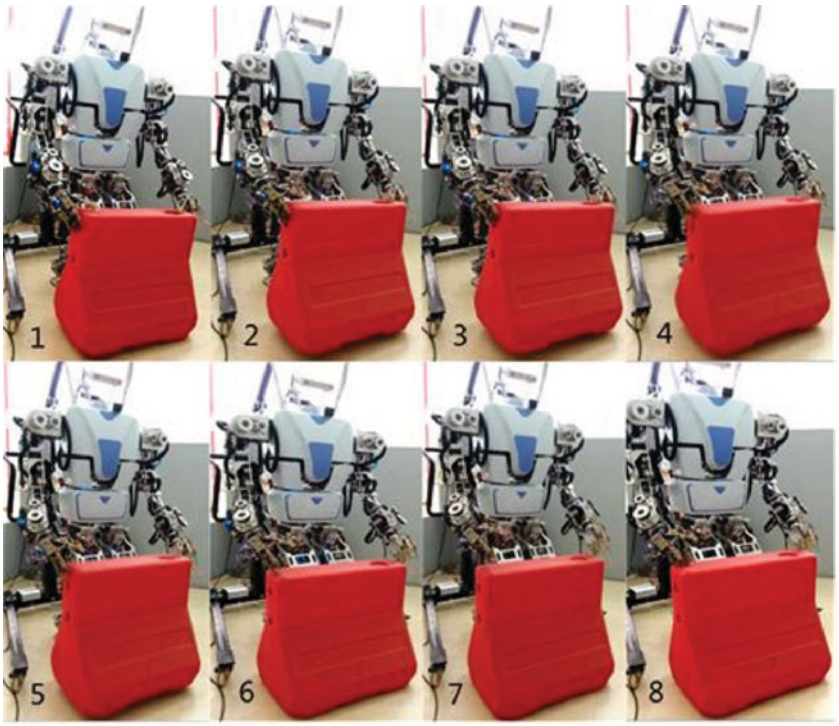

Fig. 13. The noumenon of the 7-DOF robot arm motion test process.

the error in the left arm is obvious. The fast convergence error is present on the right arm. Figure 12 shows the proposed controller for the actual interference and the NDO observations.

To demonstrate the validity of the proposed control method, the third experiment was conducted tracking the trajectory changes in moving objects on a dual-arm robot. As shown in Fig. 13, the dual-arm robot has 14 DOF, and every wrist joint is equipped with a 6D-force sensor. The manipulated object was a plastic box weighing 2000 g. Figure 5 depicts the experimental system process between the fingers and the objects at the contact spot; there was no relative movement between the ends of the fingers and the objects.

The experimental operation is described in Fig. 14. The first picture shows the initial state of the robot's arms, which have no contact with the object. The dual arm holds a roadblock off the ground and moves forward, as shown in the pictures from the second to the fifth. The sixth picture shows

https://doi.org/10.1017/S026357471800067X Published online by Cambridge University Press

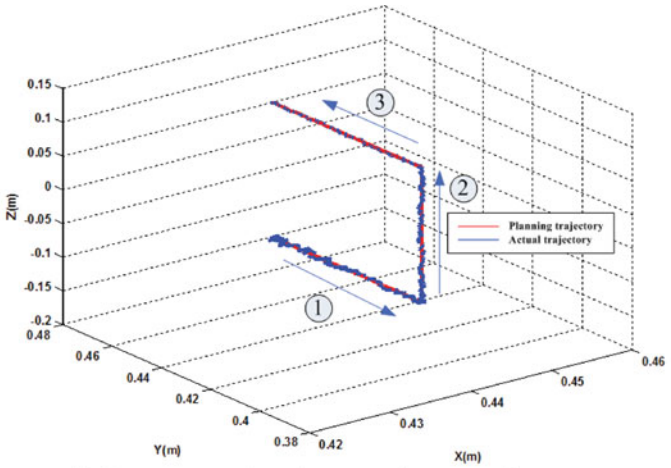

(a) Trajectory tracking changes in the moving objects

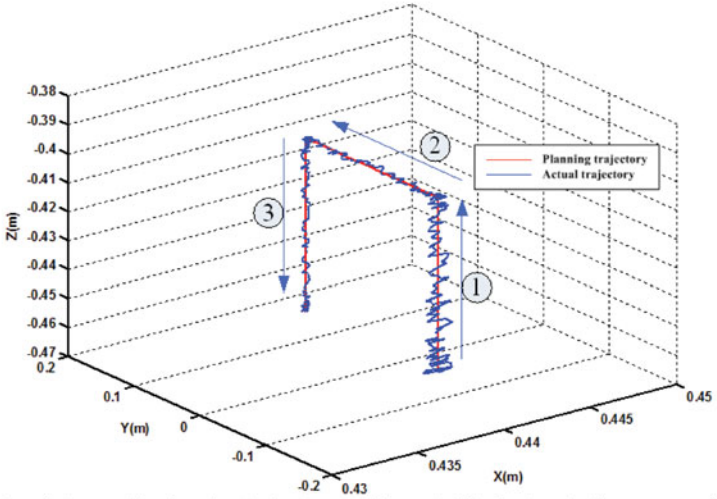

(b) Comparison between the planning trajectory and the actual trajectory in the process of moving

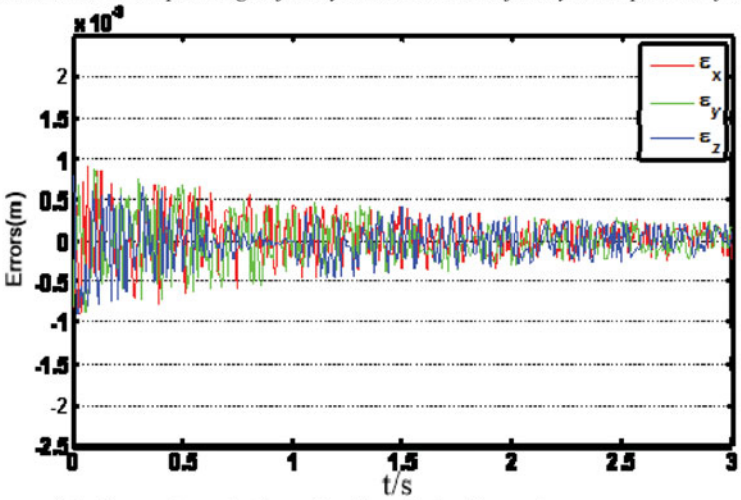

(c) Errors change in three directions during the moving process

Fig. 14. Using the proposed method in this paper, the response curve of the space motion of the dual-arm moving object. (a) Trajectory tracking changes in the moving objects. (b) Comparison between the planning trajectory and the actual trajectory in the process of moving. (c) Errors change in three directions during the moving process.

https://doi.org/10.1017/S026357471800067X Published online by Cambridge University Press

the double arm posture of the robot when the roadblock is lowered. According to the analysis of the recorded data of the right arm, we set its starting, intermediate, and end coordinates to (0.44,460,0.1), (0.44,400,0.1) and (0.44,400,0.1), and (0.44,460,0.1), respectively. Figure 14(a) displays the reference coordinates system of the right arm, and the errors of the actual motion and the tracking trajectory are demonstrated in Fig. 14(b) and (c).

Figure 14(a) shows the trajectory change curve of the robot in the process of object handling. Since there is a rotational transformation between the world coordinate system of the robot right arm and the Matlab drawing tool coordinate system, the rotation of the X-axis is 90°. The data in Fig. 14(b) is changed from Fig. 14(a) by rotation, and its time change trend is consistent with the robot coordinate system. From Fig. 14(b), the actual trajectory tracking direction could be seen, as the arrow shows below, which indicates that the actual tracking error is large at the initial stage. However, as the tracking task continues, its actual trajectory tracking motion tends to remain stable. From the error curve of the three directions in Fig. 14(c), we can see that the change in the actual error is gradually convergent. The fluctuation in the diagram is due to the high accuracy of the NDI dynamic measurement system, which captures tiny vibrations. Therefore, its actual error curve is jittering, but its overall trend is convergent.

A conclusion could be drawn from the experimental results that the control method proposed in the application of the dual-arm robot can effectively grab the object. The position and posture of the object in the free motion space can be quickly converged, and the motion error converges to a small neighbourhood near the origin, and the position error is very small. However, when the large object is moved, the time is shorter because of the lack of friction between the finger and the object.

5. Conclusion

This paper proposed the ABSMC algorithm for the dual arm of humanoid robots using an NDO. This algorithm was used to offset the bounded uncertainties because these types of robots in kinematic and dynamic models inevitably contain un-modelled dynamics, parameter uncertainties, and external disturbances. In addition, the use of the NDO matched the disturbance observation to reduce the total interference of the system, thereby weakening the chattering of the SMC. The controller did not need to generate any robot kinematic or dynamic models of the regression matrix. In addition, the controller proposed in this paper ensured that all the signals in the closed-loop system were the index of convergence, and the tracking error was uniformly and ultimately bounded. The paper also verified the use of the proposed controller for tracking performance applicability of humanoid robotic arms. Finally, the compensation controller with PID control and the repetitive control scheme were compared.

Acknowledgments

This work was supported by a project of the research fund for PhD of Southwest University of Science and Technology (Grant No. 17zx7157). Friends and former colleagues at TF-SWUFE were acknowledged for fruitful discussions on the robotic control and application.

References

1. D. Tonke and T.-E. Lee, "Modeling, analysis, and scheduling of cluster tools with two independent arms," *IEEE Trans. Autom. Sci. Eng.* **13**(2), 1176–1188 (2016).
2. S. Y. Shin and C. H. Kim, "Human-like motion generation and control for humanoid's dual arm object manipulation," *IEEE Trans. Ind. Electron.* **62**(4), 2265–2276 (2015).
3. S. J. Phee, S. C. Low, P. Dario and A. Menciassi, "Tendon sheath analysis for estimation of distal end force and elongation for sensorless distal end," *Robotica* **28**(7), 1073–1082 (2010).
4. T. Li and M. Ceccarelli, "Design and simulated characteristics of a new biped mechanism," *Robotica* **33**(1), 1568–1588 (2015).
5. D. Nicolis, A. M. Zanchettin and P. Rocco, "Constraint-based and sensorless force control with an application to a lightweight dual-arm robot," *IEEE Robot. Autom. Lett.* **1**(1), 340–347 (2016).
6. M. Ragaglia, A. M. Zanchettin, L. Bascetta and P. Rocco, "Accurate sensorless lead-through programming for lightweight robots in structured environments," *Robot. Comput.-Integr. Manuf.* **39**, 9–21 (2016).
7. J. Hill and F. Fahimi, "Active disturbance rejection for walking bipedal robots using the acceleration of the upper limbs," *Robotica* **33**(2), 264–281 (2015).

https://doi.org/10.1017/S026357471800067X Published online by Cambridge University Press

8. S. J. Huang, S. Liu and C. H. Wu, "Intelligent humanoid mobile robot with embedded control and stereo visual feedback," *J. Mech. Sci. Technol.* **29**(9), 3919–3931 (2015).
9. G. Garofalo and C. Ott, "Limit cycle control using energy function regulation with friction compensation," *IEEE Robot. Autom. Lett.* **1**(1), 90–97 (2016).
10. M. Norton, S. Khoo, A. Kouzani and A. Stojcevski, "Adaptive fuzzy multi-surface sliding control of multiple-input and multiple-output autonomous flight systems," *IET Control Theory Appl.* **9**(4), 587–597 (2015).
11. X.-H. Chang, "Robust non-fragile H_∞ filtering of fuzzy systems with linear fractional parametric uncertainties," *IEEE Trans. Fuzzy Syst.* **20**, 1001–1011 (2012).
12. F. Fahimi and C. Van Kleeck, "Alternative trajectory-tracking control approach for marine surface vessels with experimental verification," *Robotica* **31**(1), 25–33 (2013).
13. H. Liu, J. Xi and Y. Zhong, "Robust optimal attitude control of a laboratory helicopter without angular velocity feedback," *Robotica* **33**(2), 282–294 (2015).
14. W. H. Chen, D. J. Ballance, P. J. Gawthrop and J. O'Reilly, "A nonlinear disturbance observer for robotic manipulators," *IEEE Trans. Ind. Electron.* **47**(4), 932–938 (2000).
15. M. L. Corradini, V. Fossi, A. Giantomassi, S. Longhi and G. Orlando, "Discrete time sliding mode control of robotic manipulators: Development and experimental validation," *Control Eng. Pract.* **20**(8), 816–822 (2012).
16. G. P. Incremona, G. De Felici and A. Ferrara, "A supervisory sliding mode control approach for cooperative robotic system of systems," *IEEE Syst. J.* **9**(1), 263–272 (2015).
17. A. E. Firoozabadi, S. Ebrahimi and J. M. Fontllagunes, "A comparative study of elastic motions in trajectory tracking of flexible RPR planar manipulators moving with high speed," *Robotica* **35**(7), 1523–1540 (2017).
18. Q. Khan, A. I. Bhatti, M. Iqbal and Q. Ahmed, "Dynamic integral sliding mode control for SISO uncertain nonlinear systems," *Int. J. Innovative Comput. Inf. Control* **8**(7), 4621–4633 (2012).
19. A. Mohammadi, M. Tavakoli, H. J. Marquez and F. Hashemzadeh, "Nonlinear disturbance observer design for robotic manipulators," *Control Eng. Pract.* **21**(3), 253–267 (2013).
20. M. Eom and D. Chwa, "Robust swing-up and balancing control using a nonlinear disturbance observer for the pendubot system with dynamic friction," *IEEE Trans. Robot.* **31**(2), 331–343 (2015).
21. D. Ginoya, P. D. Shendge and S. B. Phadke, "Disturbance observer based sliding mode control of nonlinear mismatched uncertain systems," *Commun. Nonlinear Sci. Numer. Simul.* **26**(1), 98–107 (2015).
22. Y. Singh and M. Santhakumar, "Inverse dynamics and robust sliding mode control of a planar parallel (2-PRP and 1-PPR) robot augmented with a nonlinear disturbance observer," *Mech. Mach. Theory* **92**, 29–50 (2015).
23. S. Mohammed, W. Huo, J. Huang, H. Rifaïa and Y. Amirat, "Nonlinear disturbance observer based sliding mode control of a human-driven knee joint orthosis," *Robot. Auton. Syst.* **75**, 41–49 (2016).
24. M. Santhakumar, "A nonregressor nonlinear disturbance observer-based adaptive control scheme for an underwater manipulator," *Adv. Robot.* **27**(16), 1273–1283 (2013).
25. G. G. Rigatos, "Control and disturbances compensation in underactuated robotic systems using the derivative-free nonlinear Kalman filter," *Robotica* **35**(3), 687–711 (2017).
26. F. Abdelhedi, Y. Bouteraa and N. Derbel, "Second order sliding mode based synchronization control for cooperative robot manipulators," *Adv. Appl. Nonlinear Control Syst. Springer, Cham*, 669–683 (2016).
27. D. Zhao, S. Li, and Q Z. "Adaptive synchronised tracking control for multiple robotic manipulators with uncertain kinematics and dynamics," *Int. J. Syst. Sci.* **47**(4), 791–804 (2016).
28. K. Bai, M. Luo, M. Liu and G. Jiang, "Fuzzy Backstepping Control for Dual-Arm Cooperative Robot Grasp," *Proceedings of International Conference on Robotics Biomimetics ROBIO2015*, Zhuhai, China (Dec. 2015) pp. 2563–2568.
29. M. N. Mahyuddin, S. G. Khan and G. Herrmann, "A novel robust adaptive control algorithm with finite-time online parameter estimation of a humanoid robot arm," *Robot. Auton. Syst.* **62**, 294–305 (2014).

https://doi.org/10.1017/S026357471800067X Published online by Cambridge University Press